

## Supplementary Information

# Localized thermal spike driven morphology and electronic structure transformation in swift heavy ion irradiated TiO<sub>2</sub>nanorods

Sutapa Dey,<sup>a</sup>Anusmita Chakravorty,<sup>b</sup>Shashi Bhusan Mishra,<sup>c</sup>Nasima Khatun,<sup>a</sup>Arnab Hazra,<sup>d</sup>Birabar Ranjit Kumar Nanda,<sup>c</sup>Chandran Sudakar,<sup>e</sup>Debdulal Kabiraj<sup>b</sup> and Somnath C. Roy\*<sup>a</sup>

<sup>a</sup>. *Semiconducting Oxide Materials, Nanostructures and Tailor Heterojunction (SOMNaTH) Lab and Functional Oxide Research Group (FORG), Department of Physics, Indian Institute of Technology Madras, Chennai, India-600036.* E-mail: somnath@iitm.ac.in

<sup>b</sup>. *Inter-University Accelerator Centre, ArunaAsaf Ali Marg, New Delhi 110067, India*

<sup>c</sup>. *Condensed Matter Theory and Computational Laband Center for Atomistic Modelling and Materials Design (CAMMD), Department of Physics, Indian Institute of Technology Madras, Chennai, India-600036*

<sup>d</sup>. *Department of Electrical & Electronics Engineering, Birla Institute of Technology & Science-Pilani, Pilani Campus, Pilani-333031, Rajasthan, India*

<sup>e</sup>. *Multifunctional Materials Laboratory, Department of Physics, Indian Institute of Technology Madras, Chennai, India-600036*

**Table T1.** Some of the important published works on Ag ion irradiation effects on TiO<sub>2</sub>

Material (Reference)	Ion/Energy/Fluence	Study on/observed phenomena
Undoped and niobium doped anatase TiO <sub>2</sub> thin film <sup>1</sup>	120 MeV Ag and 130 MeV Ni ions at different ion fluence of $5 \times 10^{11}$ , $1 \times 10^{12}$ , $3 \times 10^{12}$ and $1 \times 10^{13}$ ions/cm <sup>2</sup>	A study on phase transformation
Rutile TiO <sub>2</sub> thin film <sup>2</sup>	120 MeV Ag ions at fluences from $1 \times 10^{11}$ to $2 \times 10^{13}$ ions/cm <sup>2</sup>	Micro-Raman study
Amorphous TiO <sub>2</sub> thin films <sup>3</sup>	100 MeV Ag ion beam at a fluences of $1 \times 10^{12}$ and $1 \times 10^{13}$ ions/cm <sup>2</sup> .	Rapid thermal annealing effect on SHI induced nanocrystalline thin film
Anatase TiO <sub>2</sub> thin film <sup>4</sup>	200 MeV Ag ions at fluences of $1 \times 10^{11}$ , $1 \times 10^{12}$ , and $5 \times 10^{12}$ ions/cm <sup>2</sup>	Transition from anatase to a mixed phase of brookite and rutile; changes in electronic structure observed by XAS study
Amorphous	200 MeV Ag ion at fluences from $5 \times 10^{11}$ to $10^{12}$ ions/cm <sup>2</sup>	A comparative study of thermal annealing and

TiO <sub>2</sub> thin film <sup>5</sup>	$10^{11}$ to $3 \times 10^{12}$ ions/cm <sup>2</sup>	SHI induced structural evolution. SHI leads to a structural evolution from anatase phase to pure rutile
Amorphous TiO <sub>2</sub> thin film <sup>6</sup>	100 MeV Ag ion beam at fluences of $1 \times 10^{12}$ and $1 \times 10^{13}$ ions/cm <sup>2</sup>	Formation of nano-hillocks, amorphous to crystalline phase transition
Amorphous TiO <sub>2</sub> thin film <sup>7</sup>	100MeV Ag ion at a fluence of $1 \times 10^{12}$ ions/cm <sup>2</sup>	Nano crystallization of amorphous thin film, the amorphous unirradiated PLD film containing small amount of rutile phase is recrystallized to anatase phase after SHI irradiation

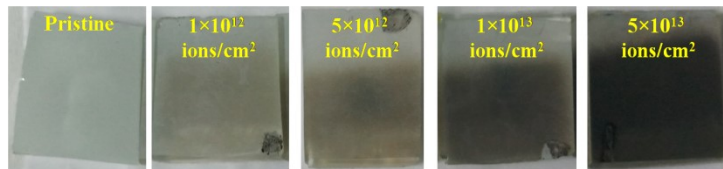


**Fig. S1.** Digital photographs of pristine and irradiated samples at different fluences

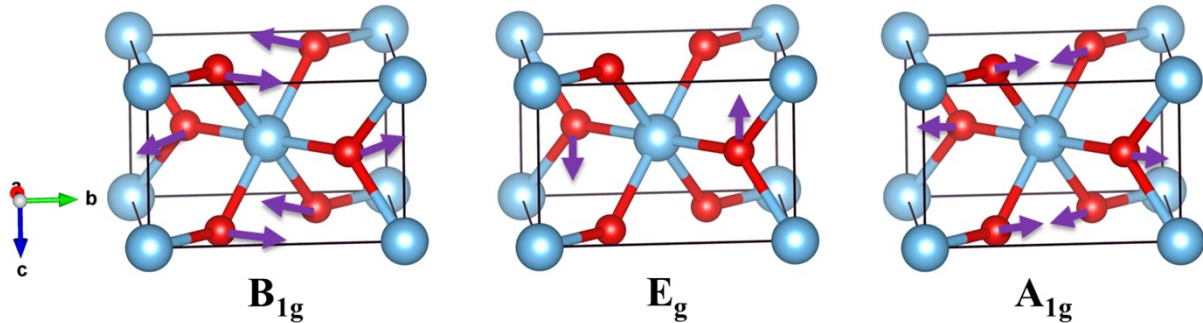


**Fig. S2.**Schematic of the vibrations of oxygen atoms corresponding to Raman modes in rutile TiO<sub>2</sub>.<sup>8</sup> The Ti and O atoms are represented by light blue and red solid spheres, respectively.

### Ion energy selection

To estimate the electronic/inelastic ( $S_e$ ) and nuclear/elastic ( $S_n$ ) energy loss by the incident ion beam, simulations based on SRIM code<sup>9</sup> were executed, and the results are presented in Fig.S3. It is observed from Fig.S3(a) that  $S_e$  dominates in the incident energy range upto 10<sup>3</sup> MeV with a

maximum value at around 300 MeV. However, for 100 MeV Ag ions interacting with TiO<sub>2</sub>, the value of S<sub>e</sub> is 19.82 keV/nm, which is more than two orders of magnitude higher than the S<sub>n</sub> (0.09 keV/nm). The S<sub>e</sub> and S<sub>n</sub> values of the 100 MeV Ag ion along the depth inside TiO<sub>2</sub> are presented in Fig.S3(b). It is observed that the S<sub>e</sub> and S<sub>n</sub> values remain almost constant along the depth (1 μm long TiO<sub>2</sub> nanorods as observed in SEM images).

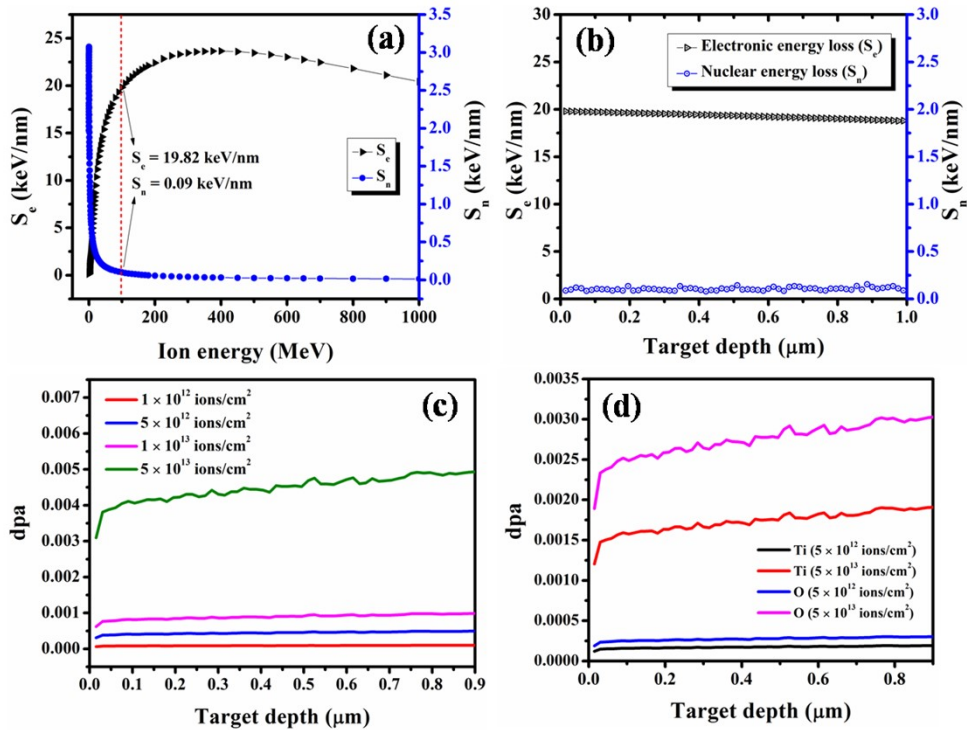


**Fig.S3.** (a) Electronic/inelastic (S<sub>e</sub>) and nuclear/elastic (S<sub>n</sub>) energy losses in TiO<sub>2</sub> as a function of incident Ag ion energy, (b) the depth profile of S<sub>e</sub> and S<sub>n</sub> in TiO<sub>2</sub> irradiated with 100 MeV Ag ion simulated with the SRIM 2013 code,<sup>9</sup> (c) total vacancies per volume, and (d) the titanium and oxygen vacancies per volume along the depth at different fluences of 100 MeV Ag ion irradiation estimated using TRIM full cascade simulation.<sup>9</sup>

The number of vacancies created at different fluences was also estimated from TRIM full cascade simulation.<sup>9</sup> This was expressed as the ratio of the number of atoms displaced over the

total number of atoms in a certain volume of TiO<sub>2</sub>. Fig.S3(c) presents the displacement per atom (*dpa*) along the length of the nanorod, which shows a gradual increment in the vacancy distribution with increasing fluence along with a stable depth profile. The estimation reveals a *dpa* of 0.005 representing 5 vacancies per 1000 atoms created in TiO<sub>2</sub> at the highest fluence of 5 × 10<sup>13</sup> ions/cm<sup>2</sup>. TRIM simulation also demonstrated a higher concentration of oxygen vacancies compared to that of titanium, which is presented in Fig. S3(d).

**Table T2.** Physical parameters of rutileTiO<sub>2</sub> for i-TS calculation

Parameters	Values for rutile TiO <sub>2</sub> <sup>10,11,12</sup>
Density for solid (g/cm <sup>3</sup> )	4.25
Density for liquid (g/cm <sup>3</sup> )	3.21
Specific heat of electron (J/cm <sup>3</sup> .K)	1
Thermal conductivity of electron (J/cm K sec)	2
Specific heat of lattice (J/g.K)	$C_a(T) = 0.96072 - 1.15732 \times e^{(-0.00482 \times T)}$
Thermal conductivity of lattice (J/cm K sec)	$K_a(T) = 0.03215 + 0.2836 \times e^{(-T/200)}$
Latent heat of fusion (J/g)	838.07
Melting point (T <sub>m</sub> ) in K	2130
Latent heat of vaporization (J/g)	6157.0
Boiling point (T <sub>b</sub> ) in K	3200
Electron-phonon mean free path (nm)	5.8

## REFERENCES

- 1 S. K. Gautam, A. Chettah, R. G. Singh, S. Ojha and F. Singh, *Nucl. Instruments Methods Phys. Res. B*, 2016, **379**, 224–229.
- 2 S. K. Gautam, F. Singh, I. Sulania, R. G. Singh, P. K. Kulriya and E. Pippel, *J. Appl. Phys.*, 2014, **115**, 143504.
- 3 M. Thakurdesai, D. Kanjilal and V. Bhattacharyya, *Appl. Surf. Sci.*, 2012, **258**, 7855–7859.
- 4 S. Gautam, K. H. Chae, H. Thakur, R. Kumar, P. Thakur, N. B. Brookes and K. K. Sharma, *J. Appl. Phys.*, 2011, **110**, 083718.
- 5 H. Rath, P. Dash, T. Som, P. V. Satyam, U. P. Singh, P. K. Kulriya, D. Kanjilal, D. K. Avasthi and N. C. Mishra, *J. Appl. Phys.*, 2009, **105**, 074311.
- 6 M. Thakurdesai, D. Kanjilal and V. Bhattacharyya, *Appl. Surf. Sci.*, 2008, **254**, 4695–4700.
- 7 M. Thakurdesai, A. Mahadkar, D. Kanjilal and V. Bhattacharyya, *Vacuum*, 2008, **82**, 639–644.
- 8 Y. Zhang, C. X. Harris, P. Wallenmeyer, J. Murowchick and X. Chen, *J. Phys. Chem. C*, 2013, **117**, 24015–24022.
- 9 J. F. Ziegler, M. D. Ziegler and J. P. Biersack, *Nucl. Instruments Methods Phys. Res. Sect. B Beam Interact. with Mater. Atoms*, 2010, **268**, 1818–1823.
- 10 K. Awazu, X. Wang, M. Fujimaki, T. Komatsubara, T. Ikeda and Y. Ohki, *J. Appl. Phys.*, 2006, **100**, 044308.

- 11 P. Zhai, S. Nan, L. Xu, W. Li, Z. Li, P. Hu, J. Zeng, S. Zhang, Y. Sun and J. Liu, *Nucl. Instruments Methods Phys. Res. Sect. B Beam Interact. with Mater. Atoms*, 2019, **457**, 72–79.
- 12 J. H. O'Connell, G. Aralbayeva, V. A. Skuratov, M. Saifulin, A. Janse Van Vuuren, A. Akilbekov and M. Zdorovets, *Mater. Res. Express*, 2018, **5**, 055015.